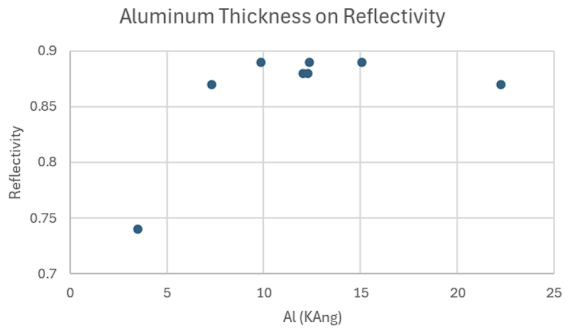

Figure 8.87: All coating from sample 10 to sample 16 with its reflectivity plotted against its aluminum thickness

8.3.4.3 The high performance DIRC

Requirements

Requirements from physics: The PID system in the central section of the ePIC detector must provide at least 3 standard deviations of separation of π/K up to 6 GeV/c, and contribute to low momentum e/π identification.

Requirements from Radiation Hardness: The anticipated radiation dose in the hpDIRC optics and its potentially sensitive readout electronics are predicted to be modest. These estimates are based on minimum-bias 10×275 GeV e+p events from PYTHIA. The maximum machine luminosity over a six-month period of annual operation at 100% machine and detector efficiency for a total of 10 years was assumed. Under these conditions, the total dose from electromagnetic and hadronic radiation is expected to be less than 100 rad. The 1-MeV-neutron-equivalent fluence is expected to reach 10^{10} neutrons per cm^2.

Requirements from Data Rates: The expected hit rate of 25 kHz per cm^2 for the hpDIRC was estimated using detailed Geant4 simulations, incorporating the Pythia event generator. This estimation assumes the baseline MCP-PMT sensors, which typically have a dark count rate of approximately 1 kHz per mm^2, or 0.09 kHz per pixel.

Justification

Device concept and technological choice: A radially compact detector based on the DIRC (Detection of Internally Reflected Cherenkov light) principle, a specialized type of RICH counter, is appropriate. It employs solid, long, rectangular-shaped radiators made of synthetic fused silica, which also serve to guide the Cherenkov photons to outside the central region for readout. This design allows the active radiator section to remain radially compact, minimizing its impact on the performance of neighboring systems and simplifying the system integration.

The photons are recorded by an array of pixelated photon sensors mounted on the back of the expansion volume. As a result of the excellent optical finish of the optical components, the emission

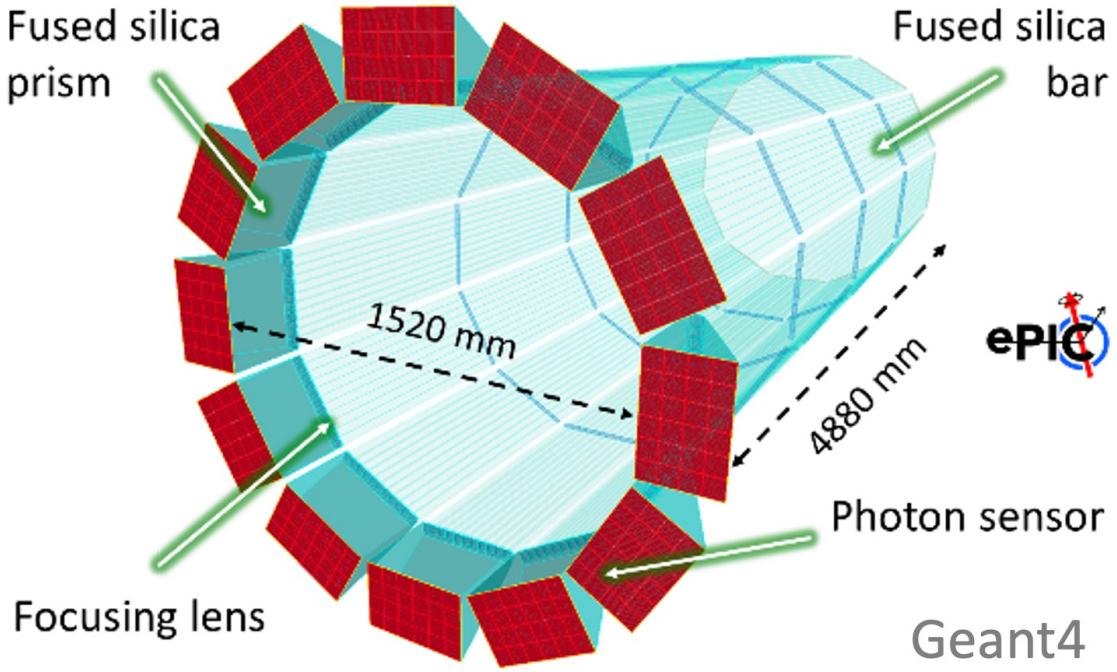

Figure 8.88: ePIC hpDIRC geometry in the Geant4 standalone simulation.

angle of Cherenkov photons with respect to the particle track is maintained during the photon transport via the total internal reflection. This angle can be reconstructed for each track from the measured position of the photon on the detector surface and the measured arrival time of each photon.

The general concept of a barrel DIRC detector was first successfully demonstrated by the BaBar DIRC and followed by several other experiments worldwide. The ePIC high-performance DIRC (hpDIRC) takes advantage of the lens-based focusing concept of the PANDA Barrel DIRC, and has also several other advancements to meet the performance requirements of the Electron-Ion Collider (EIC). The hpDIRC concept for ePIC was developed as part of the EIC generic R&D program performed by the EIC PID collaboration (eRD14) and direct EIC Project R&D eRD103 with the focus on extending the momentum coverage well beyond the DIRC counter state-of-the-art at that time.

Subsystem description:

General device description:

The baseline design of the ePIC hpDIRC detector, as implemented in a detailed and test beam-vetted Geant4 simulation, is shown in Fig. 8.88. It is divided into twelve optically isolated sectors, each composed of a bar box and a readout box. These 12 sectors surround the beamline in a 12-sided polygonal barrel with an inner radius of about 760 cm. Each bar box includes ten radiator bars, each made of synthetic fused silica and with a length of 4880 mm and a cross-section of 17 mm $\times$ 35 mm. The bars are placed side-by-side, separated by small air gaps, inside the light-tight bar box. Mirrors are attached to one end of each bar to reflect the Cherenkov photons towards the other (readout) end. At the readout end they exit the bar and are focused by a 3-layer spherical lens on the back surface of the prism which

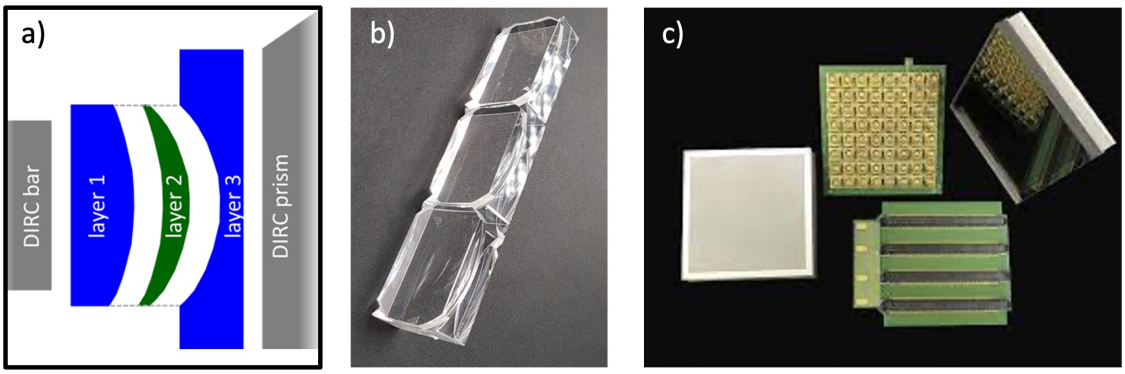

Figure 8.89: a) Schematic of the side view of one hpDIRC section and an exploded view of the 3-layer lens. b) Photo of prototypes of the 3-layer spherical lenses. c) Photec AuraTek MAPMT253.

serves as an expansion volume.

Bars:

The baseline ePIC hpDIRC design envisions that the 120 long bars needed will be composed of three repurposed BaBar DIRC bars and one shorter new bar manufactured by industry. The number of bar boxes and bars per box has been optimized to the width of the BaBar DIRC bars while maximizing the azimuthal acceptance of the hpDIRC. This approach assumes that the BaBar bars can be safely extracted from the Babar boxes without compromising their optical and mechanical integrity. The disassembly and evaluation of the BaBar bar boxes are currently underway. Final information on the availability of Baber bars for ePIC is expected by Spring 2025.

Lenses:

The 3-layer spherical focusing lens is a novel component of the hpDIRC and is essential for achieving the PID performance ePIC requires. The lens design, shown in Fig.8.89, avoids the dramatic photon loss caused by air gap transitions in standard lens systems. It does this by focusing Cherenkov light through refraction at the interface between synthetic fused silica and a high-refractive-index material, such as sapphire or lanthanum crown glass. A thin layer of the high-refractive-index material is sandwiched between two layers of synthetic fused silica, with carefully optimized radii of curvature on all spherical surfaces. This design combines defocussing and focusing transitions to form a flat detector plane that accommodates a wide range of photon angles, matching the layout of the sensor array on the expansion volume prism. Several prototypes using different materials for the middle layer have been produced by the optical industry, and examples of these three prototypes are shown in Fig.8.89b.

Prisms:

The prism expansion volume is made of synthetic fused silica, has a 32° opening angle, and dimensions of 237 mm × 350 mm × 300 mm. The detector plane of each prism is covered by an array of 24 sensors shown in red in Fig. 8.88.

Sensors:

The photosensors attached to the rear of the prism record the positions and arrival times of the Cherenkov photons. In the baseline design of the hpDIRC, commercial microchannel plate photomultiplier tubes (MCP-PMTs) with a pore size of 10 µm or smaller were as-

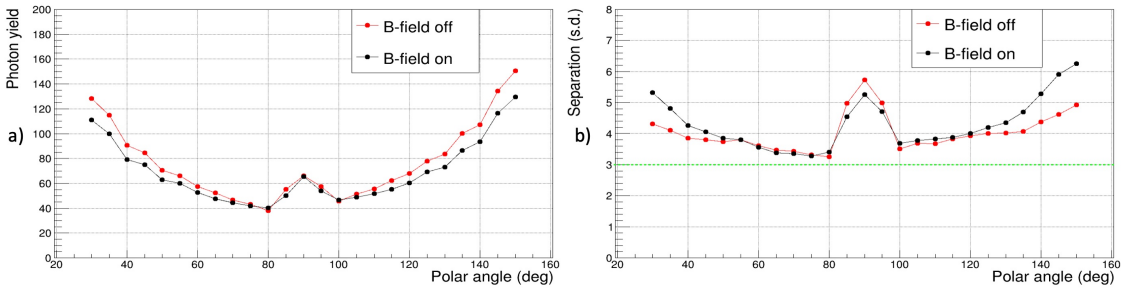

Figure 8.90: The expected performance of the hpDIRC as a function of the particle's polar angle in terms of photon yield (a) for pions and π/K separation power (b). These results are based on a standalone Geant4 simulation of 6 GeV/c particles.

sumed. A pixel size of 3.2 mm was chosen based on Geant4 simulations as a balance between cost, performance, and expected availability as the sensor technology for the hpDIRC. Lifetime-enhanced 2" MCP-PMT tubes are commercially available from Photonis and Photek with suitable DC-coupled anode configurations. The simulation utilized Photonis Planacon XP85122 MCP-PMTs, incorporating realistic sensor characteristics including photon timing, collection efficiency, and quantum efficiency. With the termination of the production of the Photonis PMTs, the Photek MAPMT 253 sensors shown in Fig. 8.89 are now the leading candidates for the hpDIRC. These share the same footprint and are expected to exhibit similar properties to the Photonis tubes.

FEE: Fast ASIC-based readout systems are being developed by the EIC project to meet the demands of various ePIC detector systems. For the hpDIRC, the readout electronics must be capable of detecting small signals (on the order of a few millivolts) from MCP-PMTs while maintaining excellent single-photon timing resolution. Additionally, the electronics need to match the channel density and sensor footprint, as they will be directly coupled to the back of the sensor to minimize distance and achieve optimal timing precision. The two leading candidates for hpDIRC readout are EICROC and FCFD, which are discussed in detail in Section XXX.

Performance Figure 8.90 presents the expected performance based on standalone Geant4 simulation studies. The plots illustrate particles that are fired over a range of polar angles but with an azimuthal angle fixed at zero degrees (so perpendicular to one of the middle bars). The black points represent the photon yield and separation power for 6 GeV/c charged pions and kaons as a function of polar angle with the magnetic field enabled, while the red points display the same data with the magnetic field disabled.

The number of detected Cherenkov photons per particle (plot a) ranges from 40 to 150, depending on the polar angle. The sharp increase in photon yield at steeper forward and backward angles is due to the longer track lengths in the fused silica bars, with an asymmetry in forward/backward yields resulting from photon loss along longer propagation paths at smaller polar angles. The peak in the photon yield near a polar angle of 90° occurs because a larger fraction of the photons satisfy the total internal reflection criterion near perpendicular incidence, compared to slightly larger or smaller angles.

The "separation power" for both particle hypotheses (plot b) is obtained from Gaussian fits to the log-likelihood differences between pairs of particle hypotheses. It is calculated as the difference between the means of the two Gaussians divided by the arithmetic average of the two widths. The

slightly improved performance for polar angles above 100° is due to shorter photon paths, resulting in higher photon yields and reduced chromatic dispersion in the bar material.

Similar studies were conducted for electron-pion (e/π) separation, which is primarily the responsibility of the Electromagnetic Calorimeter. However, the hpDIRC can further improve the performance at low momentum. At lower momenta, multiple scattering is severe, but assuming ePIC achieves the tracking resolution described in the Yellow Report, the hpDIRC can provide a 3 standard-deviation separation power up to 1.2 GeV/c. The expected particle identification (PID) performance of the hpDIRC thus surpasses the ePIC PID goal, achieving more than 3 standard deviations of separation power for e/π identification up to 1.2 GeV/c and π/K separation up to 6 GeV/c across the entire polar angle range.

Performance Systematic Studies Most of the hpDIRC performance studies were conducted using a particle gun, providing precise control over the parameters under investigation while covering the entire required angular and momentum ranges. Detailed studies examined a range of azimuthal angles to measure the performance across the full width of the bar box. While a moderate performance deterioration was observed in some of the non-central bars, the system maintained the required 3-standard-deviation separation power. The effect of the magnetic field on hpDIRC performance was found to be negligible, as confirmed through simulations that incorporated a realistic ePIC magnetic field map.

Additionally, studies using Pythia-generated physics events were performed to assess the frequency and effect of multiple tracks per event within a single bar and hpDIRC module. Even in the extremely rare cases where two or more particles are very close in momentum, polar, and azimuthal angles within a single event, the impact on performance was found to be moderate, demonstrating the robustness of the hpDIRC system.

Most studies were based on an assumed angular tracking resolution of 0.5 mrad at 6 GeV/c. However, the simulation software is prepared to import and integrate a more detailed tracking parametrization when it becomes available.

Detailed hpDIRC PID Look-Up-Tables (LUTs), including the threshold mode, were generated using Geant4 simulations. These LUTs are now employed to streamline physics analyses without the need for full reconstruction.

Simulation tools and validation A detailed standalone Geant4 simulation, featuring realistic geometry and material properties, was developed in collaboration with the PANDA Barrel DIRC group and validated through modular prototype tests using particle beams at CERN. The simulation incorporates measured values for MCP-PMT quantum efficiency, collection efficiency, and timing resolution. It also accounts for the coefficient of total internal reflection of the DIRC radiator bars as a function of photon energy, the bulk transmission of the bars, glue, and lenses, as well as the wavelength-dependent refractive indices of the materials used, the photocathode, and the reflectivity of the mirrors. Background contributions from hadronic interactions and delta electrons in the bar, along with effects from MCP-PMT dark noise and charge sharing between anode pads, were also simulated.

All relevant resolution factors for hpDIRC performance are modeled using Gaussian smearing with conservative resolution assumptions. The total timing precision per photon, including sensor and readout electronics, is assumed to be 100 ps, and the angular resolution of the ePIC tracking system at the hpDIRC radius is assumed to be 0.5 mrad for particles with a momentum of 6 GeV/c.

Figure 8.91 presents photos of the modular PANDA Barrel DIRC prototype along with results ob-

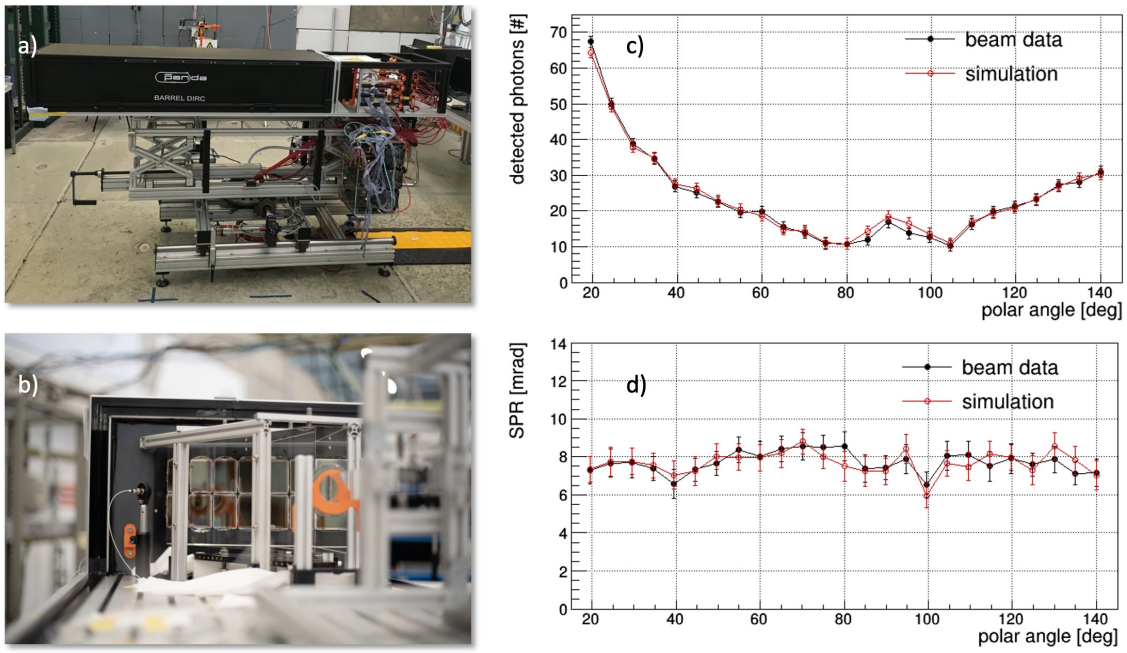

Figure 8.91: Photographs of the PANDA Barrel DIRC prototype (a), including a close-up of the readout section (b) taken during the CERN test beam. Performance plots illustrate the comparison between simulated and experimental data for photon yield (c) and single photon Cherenkov angle resolution (SPR) (d).

tained during the 2018 test beam campaign at CERN. Although the PANDA prototype differs significantly from the ePIC hpDIRC in terms of geometry (single bar), slower readout electronics, and lower-quality sensors with larger pixels, the studies and results are highly valuable for hpDIRC development. The same software used for all ePIC hpDIRC performance studies was employed to successfully reproduce the PANDA prototype test beam results. As shown in Fig. 8.91c and d, the agreement between the simulation and experimental data is excellent

Reconstruction methods The hpDIRC utilizes two primary reconstruction methods for identifying particles based on Cherenkov photon detection: geometric reconstruction and time-based imaging reconstruction. These methods translate the detected photon patterns into meaningful physical information, particularly the Cherenkov angle, which allows direct particle identification.

Geometric reconstruction in DIRC detectors is based on determining the Cherenkov photon direction from the mutual location of the radiator's readout end and the pixel hit by the photon. This method allows direct geometrical reconstruction of the Cherenkov angle for each detected photon by utilizing both the photon's direction and the beam particle's direction. Photon directions in the prism are pre-calculated using full simulations, taking into account the optical materials, and stored in look-up tables (LUT). Discrete ambiguities arise due to photon reflections within the optical system, but these can be reduced by applying a cut on the difference between the expected and measured photon arrival times. The geometric method relies on the photon position, and only uses timing information to suppress background noise. The geomtrical method also provides key performance variables such as the single-photon Cherenkov angle resolution and the yields of signal and background photons.

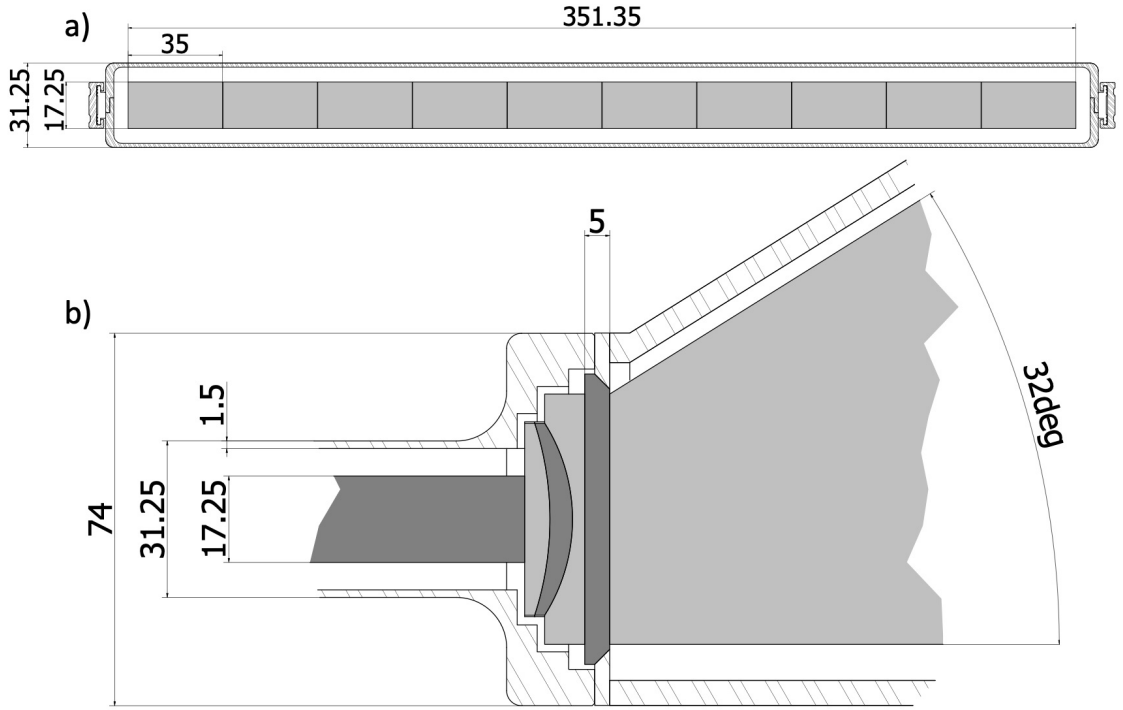

Figure 8.92: Technical drawings of the ePIC hpDIRC detector, showing the XY cross-section of the bar box (a) and the YZ cross-section of the connection between the bar box and the readout box (b).

The time-based imaging reconstruction method greatly enhances the particle identification (PID) by fully utilizing both the timing and position information of the detected photons. This method compares the measured photon arrival times against expected distributions for each particle hypothesis, stored as probability density functions (PDFs) derived from experimental or simulated data. For each photon, a time-based likelihood is calculated, which is then combined with the Poissonian PDF of the number of detected photons to provide the likelihood. Unlike the geometric reconstruction, the time-imaging method is suitable for both narrow-bar and wide-plate radiators, offering better separation power between the particle species. This method achieves the best resolution and allows for the most effective corrections of distortions.

Implementation

Subsystem mechanics and integration: The hpDIRC consists of two primary sub-assemblies: the readout section and the bar section. Both sections are composed of 12 boxes made of carbon fiber reinforced polymer (CFRP), with varying thickness depending on the stresses expected in different regions.

The readout section includes the fused silica expansion prism, readout sensors, and front-end electronics. The expansion prism has an angle of 32° and maximum dimensions of 300 mm in length, 352 mm in width, and 237.5 mm in thickness. The MCP-PMTs are coupled to the 352 mm x 237.5 mm back face of the prism using an optical interface. The sensors and associated readout electronics are mounted onto a 3D-printed frame. The rear of the readout box is sealed with a light-tight

plate with ports for cables, fibers for calibration lasers, and monitoring cameras. Dry nitrogen gas is flowed through the readout box to keep the prism's surface clean and free from dust and condensation. To maintain stable temperatures and cool the electronics, water circulates through tubing thermally coupled to the heat sources.

The bar box is composed of a top and bottom shell with overall dimensions of 4627 mm in length, 368 mm in width, and 31.25 mm in height. Figure 8.92a shows a dimensioned view of the XY cross-section of the hpDIRC bar box. The thicker part of the carbon fiber shell on the sides will be used during installation to slide in the bar box and hold it in place. The carbon fiber thickness is 1.5 mm across the width and 3 mm across the height.

Each bar box contains 10 long radiator bars, lenses, and mirrors. The radiator bars are 35 mm wide, 17.25 mm thick, and 4580 mm long, spaced 0.15 mm apart using shims to ensure optical isolation. Each long radiator bar is made up of four shorter bars bonded together with an optically transparent adhesive, similar to the BaBar DIRC construction. Three of the shorter bars, each 1225 mm long, are repurposed from the BaBar experiment, while the fourth is newly manufactured to meet the ePIC total length requirement of 905 mm.

At one end of each long bar, a 3 mm-thick flat mirror reflects photons back toward the readout end. At the opposite end, a three-layer lens is attached to the bar using the same adhesive used to join the short bars. The lens-mirror-bar joints are kept in compression by adjustable spring plungers located behind the mirrors, which reduce stress on the joints and prevent movement during installation or operation. The spring system also compensates for differential thermal expansion and contraction rates between the bars and the bar box. Each short bar is supported by two pairs of fixed nylon buttons along its length, which minimize stress on the glue joints and reduce photon loss by reducing contact with the radiator surface. Eight support pairs are evenly distributed along each long bar's length, with adjustable spring buttons pressing the bars against the fixed buttons to maintain secure positioning while preserving the optical isolation. Similar support mechanisms are used for the 17.25 mm-thick end of the bars, where all 10 bars are pressed against a single set of fixed buttons. To handle the additional stress at the button locations and accommodate holes for the spring buttons, the CFRP is locally thickened at these points. Like the readout boxes, the bar boxes are also flushed with dry nitrogen to protect the radiator bars' surfaces, with nitrogen introduced at the mirror end and vented near the lenses.

The hpDIRC consists of 12 bar boxess and 12 readout boxes. The lenses at the bar box end are coupled to a thin window that seals the box, while this window is in turn connected to the prism in the readout box using an optical interface during final installation. The readout box, including the prism, is compressed against the bar box window to form a tight optical seal. Figure 8.92b is a dimensioned view of the XZ cross-section of the connection between the bar box and the readout box. The 5 mm thick window between the 3-layer lens and the prism represents an initial design, which may be adjusted following further studies of strains and forces acting on the system.

The hpDIRC is positioned radially just inside the Barrel Electromagnetic Calorimeter (EM Calorimeter) and just outside the outer Micro-Pattern Gas Detector (MPGD) within the ePIC detector. Both the bar boxes and the MPGD are supported by the EM Calorimeter via rails mounted on triangular brackets extending radially inward from the calorimeter's inner surface.

Installation: During installation, the bar boxes are placed on a specialized lifting fixture, allowing them to be rotated into their final orientation before being transferred along rails into their designated positions. The readout boxes are supported by an external ring attached to the Hadron Calorimeter via a series of legs. Each readout box is aligned with its corresponding bar box using specialized brackets and rails, which allow the readout box to be slid into position, compressing

the optical interface and forming the connection. This rail system also enables the readout boxes to be removed without disturbing the bar boxes if necessary.

Services: Gas and Moisture Control: To maintain a low-moisture environment for the bars, dry nitrogen gas from liquid nitrogen boil-off will flow through each box. The nitrogen gas will be monitored for humidity and filtered through a molecular sieve and mechanical filters to remove particulates. Some of the input N_2 gas will leak from the bar boxes, also helping to keep the bar box slots in the mechanical support structure free of condensation.

Power Supply and Monitoring: Both high- and low-voltage supplies will be provided for each MCP-PMT sensor. A control and monitoring system will be implemented for the readout and bar box sections. The high voltage required for each MCP-PMT will be supplied by commercially available multichannel power supply modules in crates located outside the experiment.

The low-voltage power supplies, which regulate power to the front-end electronics (FEE), need to be placed as close as possible to the detector, in racks dedicated to the hpDIRC system. A modular, multichannel approach—similar to the high-voltage system is planned for the control and monitoring of voltages, currents, and onboard temperatures for all FEE boards. The low voltage levels will range from 1 to 48 V, with currents reaching several Amperes.

Cooling System: The highly integrated FEE design generates a significant amount of heat in the compact readout unit. This heat will be extracted by a water cooling system, and the necessary supply lines are included in the mechanical design of the readout boxes, although further optimization is required.

Environmental Monitoring: Standard commercial devices will monitor environmental parameters such as temperature and humidity at various locations inside the hpDIRC volume to ensure optimal performance and safety.

Calibration, alignment and monitoring: Time Calibration: To achieve the time resolution required for the hpDIRC, it is essential to eliminate time offsets between pixels, which may arise from differences in cable lengths and pixel-to-pixel variations within the photon sensors. A laser monitoring system will be employed to provide channel-by-channel time-zero information, which will be stored in a database. This data will be used to accurately calibrate the photon arrival times for all pixels.

Optical Calibration and Alignment: The exact positioning of the optical components will be determined during the hpDIRC DIRC installation, using a laser and precise survey marks. The reconstruction of the Cherenkov angle, based on the hit pattern on the MCP-PMT array, depends on the accurate relative positions and orientations of all optical elements, including the photon sensors and their individual pixels.

In-Beam Calibration and Alignment: After installation in the ePIC detector, the alignment of the hpDIRC will be verified using beam data. Samples of muons, pions, kaons, and protons identified by other ePIC sub-detectors or through kinematic fitting will be used to calibrate the hpDIRC's measured Cherenkov angles.

Geometric reconstruction will then be used to calculate the Cherenkov angle per photon for each track and sensor pixel. Any deviation between the measured and expected Cherenkov angles in the calibration samples will be utilized to develop a correction function or multi-dimensional lookup table. This information will be stored in the configuration database to correct for residual misalignment and optimize the performance. A similar procedure was successfully employed in the

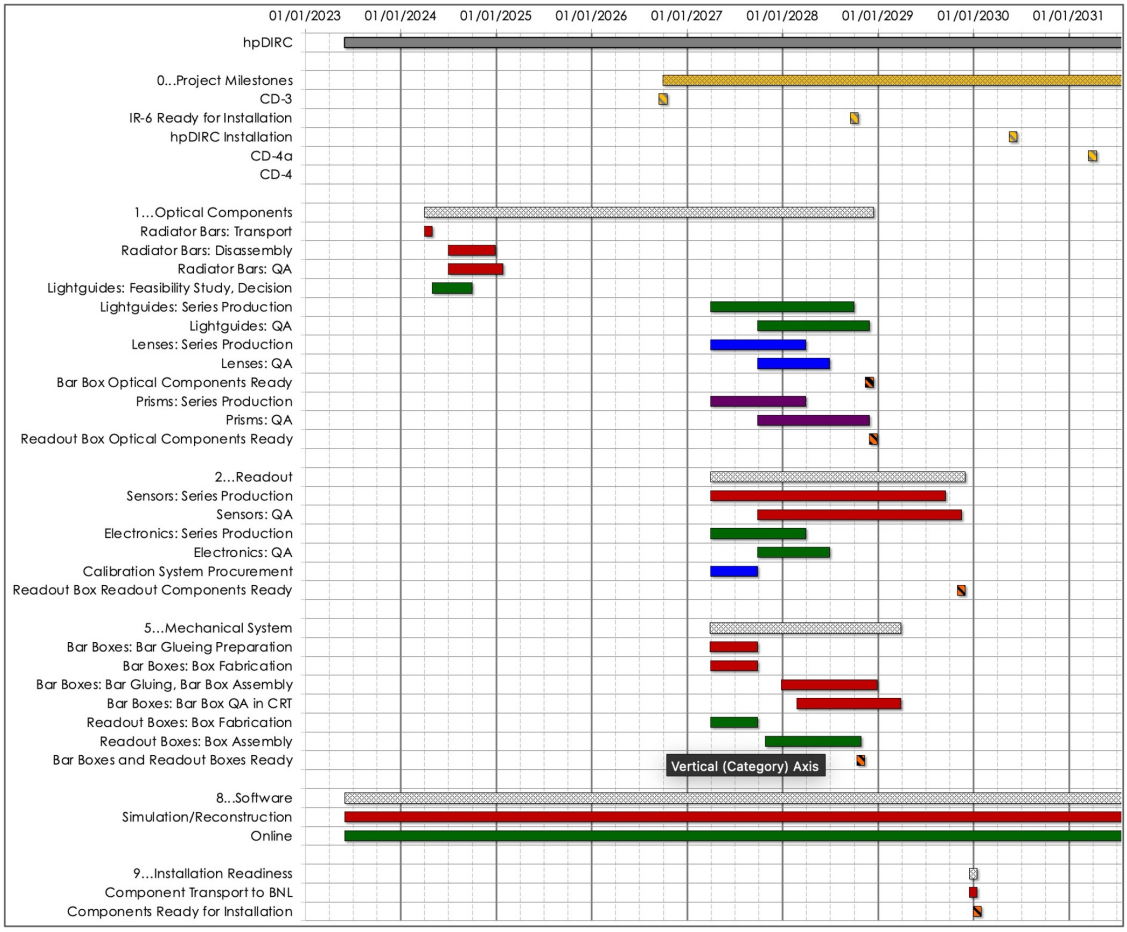

Figure 8.93: ePIC hpDIRC schedule chart alignment with EIC Project schedule

BaBar DIRC, where a 10% improvement in Cherenkov angle resolution was achieved by applying per-photon corrections based on a dedicated particle calibration sample.

Status and remaining design effort: Preparations for the hpDIRC are progressing in line with the overall project schedule. In the chart shown in Figure 8.93, the top few lines highlight the major milestones of the project from the present day to the start of the experiment and CD-4 approval. Below these milestones is a detailed breakdown of key work packages, including the optical components, readout system, and mechanical design. The hpDIRC is expected to be fully ready in advance of the installation deadline, with a substantial time contingency built into the schedule.

The length of the ePIC barrel necessitates a "light guide section" to direct photons from the active part of the hpDIRC bars to the expansion volume prism, where they are imaged. In the baseline hpDIRC design, shorter bars with the same cross-section as the narrow bars are used, as shown in Figure 8.94a for one module.

Figure 8.94b illustrates an alternative hybrid design, featuring a single wide plate in the light guide section that replaces the narrow bars. The primary motivation for this geometry was potential cost savings, but it also introduced additional opportunities. For instance, the choice of lens type

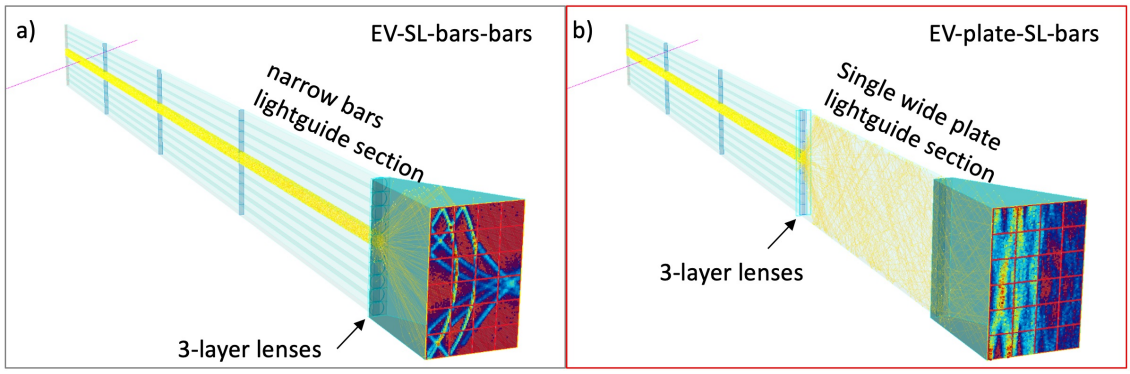

Figure 8.94: Event displays of a single module of the hpDIRC narrow bar baseline design geometry (a) and the narrow bar with wide plate hybrid geometry (b), illustrating an example of the accumulated hit pattern from charged pions, based on the standalone hpDIRC Geant4 simulation package.

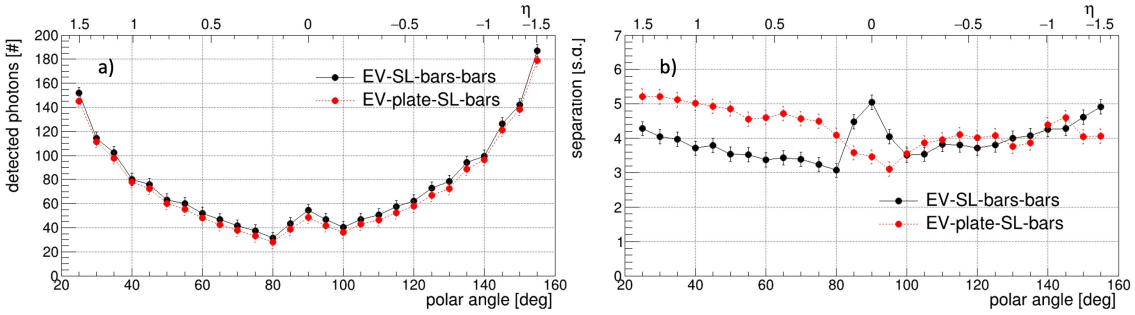

Figure 8.95: Performance comparison between the hpDIRC narrow bar baseline design geometry (black points) and the narrow bar with wide plate hybrid geometry (red points) in case of photon yield (a) for pions and π/K separation power(b) based on a standalone Geant4 simulation for particles with a momentum of 6 GeV/c.

became a question: should it be a set of spherical lenses matching each narrow bar or a single large cylindrical lens? Furthermore, where should the lens be positioned: after the light guide section as in the baseline design, or before the prism expansion volume, or even earlier, between the narrow bars and the plate to initiate the expansion sooner?

Detailed simulation studies of these configurations led to the selection of a geometry featuring a set of spherical 3-layer lenses with an optimized shape, placed before the light-guide plate, as the leading candidate for the alternative design. Figure 8.95 compares the performance of this alternative design (red points) with the baseline design (black points). The wide plate alternative shows a significant performance improvement for particle tracks with polar angles below 80°, comparable performance for polar angles above 100 degrees, and a slight reduction in performance for tracks around 90° and above 145°s. Despite these reductions, the separation power in the lower-performance regions remains above the required 3 standard deviations, making this hybrid design a promising alternative. However, this geometry has not yet been experimentally validated and would require further investigation before it could replace the current baseline design.

Remaining R&D effort: The primary objectives of the remaining hpDIRC R&D are to validate new, untested components, ensure their successful integration into the hpDIRC system, and to optimize the final design. Ultimately, the goal is to achieve a validated, cost-efficient hpDIRC design for the ePIC detector, which will be demonstrated through a vertical-slice prototype in the Cosmic Ray Telescope (CRT) setup. Several critical aspects of the hpDIRC design still require thorough study and verification to guarantee the necessary performance, mitigate risks, and explore new opportunities.

Additional R&D projects with a direct impact on the hpDIRC include eRD109 (focused on readout and ASIC designs) and eRD110 (focused on photosensors). The development of compact readout electronics for fast single-photon detection, using high-density sensors, must be completed and integrated into the hpDIRC prototype to validate the performance of a cost-optimized design for particle identification (PID).

The final hpDIRC prototype will assess the optimized sensor arrangement and explore a potential new focusing approach within a hybrid design, as shown in Fig. **??**, which combines a narrow bar with a wide plate. This configuration offers significant cost-reduction potential, but it has not yet undergone experimental testing. Additionally, the reuse of BaBar DIRC bars, another key cost-saving measure, is currently being explored with support from Jefferson Lab and the EIC Project, as discussed above.

Environmental, Safety and Health (ES&H) aspects The hpDIRC system is designed to operate without the use of any flammable gases or cryogenic liquids, which eliminates the risks associated with these hazardous substances. Both the bar boxes and readout boxes will be purged using boil-off dry nitrogen, which will flow at a rate of a few liters per hour per box. This method ensures that the environment inside the boxes remains dry and free from contaminants, contributing to the system's safety and reliability.

In terms of electrical hazards, the sensors employed in the hpDIRC require high voltages, reaching up to 2.5 kV. To prevent the risk of electrical shock, the high-voltage (HV) connections will be completely inaccessible during normal operation. Furthermore, the HV module will be keyed off, ensuring that only trained personnel will be allowed to operate it, providing an additional layer of safety in the system's design.

The hpDIRC will also utilize a class 3B Helium-Cadmium (HeCd) laser pulser for the calibration of sensors and electronics. Since lasers pose a radiation hazard, special precautions will be taken: the laser will be fully enclosed within optical fibers to prevent exposure, and only trained personnel will be authorized to operate the laser.

For the cooling of the readout electronics, a chilled liquid will be used, though the specific details of the liquid have yet to be determined. To avoid the risk of a chemical leak, the cooling liquid will circulate at sub-atmospheric pressure, which helps prevent potential leaks.

The entire hpDIRC system will comply with all applicable Environment, Safety, and Data (ES&D) standards and Occupational Safety and Health Administration (OSHA) regulations. This commitment to compliance ensures that the system adheres to the highest safety protocols, protecting both the equipment and the personnel involved in its operation.

Quality Assessment (QA planning: The quality assurance (QA) plans for the hpDIRC components and modules prior to construction are centered around a combination of process control at the vendor sites and extensive in-laboratory measurements. The radiator bars and light guides will undergo vendor-provided QA to assess their mechanical properties. Following this, a laser

Figure 8.96: Photos of available setups developed during the hpDIRC R&D program that will be used for future QA of 3-layer lenses with laser setup at ODU (a), bars and other optics at Jefferson Lab (b) and readout chain including sensors and electronics and other hpDIRC components in hpDIRC prototype at CRT at SBU (c).

scanning system at JLab will be used to monitor the internal photon transport efficiency of either the repurposed BaBar DIRC bars or the newly produced DIRC bars. This will directly ensure that the optical performance of the bars meets the ePIC DIRC standards.

For the sensors and electronics testing, laser pulser systems will be deployed at CUA, JLab, or USC (to be determined) to perform measurements including gain, quantum efficiency, collection efficiency, and dark count rate. These tests will verify the operational integrity and performance of the sensors.

The lenses will be evaluated at the laser laboratory at ODU, where the shape of the focal plane will be carefully analyzed to ensure proper optical alignment and focusing. Prisms will be subjected to vendor-provided QA, followed by further checks at WSU to confirm their specifications. Similarly, the bar boxes and prism boxes will undergo QA at the vendor sites, with additional testing and validation at SBU.

Once the DIRC modules are fully assembled, including the coupling of the bar box to the readout box (a vertical slice), the Cosmic Ray Telescope at SBU will be used for testing. This will ensure that the assembled DIRC modules function as intended before final integration.

After installation of the DIRC module in ePIC, a picosecond laser pulser calibration system will be employed to fine-tune the system. Cameras will also be used to continuously monitor the optical coupling between the sensors, prisms, and lenses, ensuring that the entire optical system is correctly aligned and operational throughout the experiment. These comprehensive QA measures are critical to ensuring the high-performance operation of the hpDIRC system in the ePIC experiment.

Construction and assembly planning: In the current plan for the ePIC hpDIRC construction, the assembly will take place at three different locations. The bar boxes will be assembled at Jefferson Lab, utilizing the existing infrastructure developed for the disassembly of the BaBar bar boxes and the quality assurance of the bars. Short bars will be glued together to form ten long bars per bar box, with 3-layer lenses attached, and will then be mounted inside their carbon fiber shells. The readout boxes will be assembled at Wayne State University, incorporating newly acquired expansion volume prisms, as well as readout sensors and electronics previously validated at USC. Once both the bar boxes and readout boxes are assembled, they will be transported to BNL for initial alignment and matching before their final installation into the ePIC detector.

Collaborators and their role, resources, and workforce: The hpDIRC system collaboration (DSC) consists of a core group of institutions that have long-standing experience with DIRC counters, having contributed to the BaBar, GlueX, PANDA projects, and the EIC DIRC R&D program. Many of these groups have been involved in these efforts since 2011, bringing a wealth of expertise to the development of the hpDIRC system for the ePIC detector. This collaborative network is expected to expand, with few expressions of interest (EoIs) from various institutions interested in contributing to different aspects of the project closer towards constriction. The process of aligning expertise and interest with system priorities is already underway, ensuring that the work is distributed efficiently.

Among the key collaborators, Jefferson Lab together with CUA have been handling the transport and disassembly of BaBar DIRC bar boxes and validating the quality of the disassembled bars. They will continue this effort with the optional quality assurance (QA) of new bars or plates for the light guide section. Jefferson lab has expressed interest in continuing this support with an extension to the gluing of bars and lenses and final assembly of the bar boxes

Stony Brook University (SBU) is preparing an important QA tool with their Cosmic Ray Telescope. The initial plan is to use it for incremental integration of new components into the hpDIRC prototype like disassembled BaBar bars, sensors, and electronics, but eventually, it will be used for validation of full bar box modules. Old Dominion University (ODU) will contribute by evaluating the focal plane of the lenses and conducting QA procedures, ensuring the optical components meet the required standards.

On the sensor side, USC will handle QA and tests related to the readout chain, ensuring the sensors operate within specified parameters. Wayne State University (WSU) will oversee the assembly and QA of the readout boxes, another critical component of the system. Finally, institutions like CUA, GSI, William & Mary, and WSU are heavily involved in simulation and reconstruction efforts, which are essential for optimizing the performance and integration of the hpDIRC system into the overall ePIC detector framework.

This broad collaboration, with specific responsibilities assigned to various expert groups, ensures that all components of the hpDIRC system are developed and tested by specialists, assuming more junior workforce like graduate students and postdoctoral researchers can be added through external grants.

Risks and mitigation strategy: The disassembly of the BaBar bar boxes is in an advanced stage of preparation, with the process set to begin soon. Immediately after disassembly, the quality of the legacy BaBar bars will be evaluated to determine their suitability for use in the ePIC hpDIRC. A decision on their usability is expected by early Summer 2025. If new radiator bars are required, a vendor will need to be identified, and the procurement and production process initiated. Based on the current production timeline for PANDA Barrel DIRC radiator bars, the production of new bars

for ePIC is still possible within the project schedule.

Both the baseline commercial MCP-PMTs and HRPPDs require testing and evaluation, which are being prepared by different groups. These tests will be conducted in parallel to ensure the necessary sensors are available within the required time before installation. The development of ASIC-based readout electronics is being coordinated by the EIC project, with two parallel solutions under consideration.

Additional Material Add text here.

References

[1] A. Bacchetta, V. Bertone, C. Bissolotti, G. Bozzi, M. Cerutti, F. Delcarro, M. Radici, L. Rossi, and A. Signori, "Flavor dependence of unpolarized quark transverse momentum distributions from a global fit," *JHEP*, vol. 08, p. 232, 2024.

[2] Irene Dutta and Christopher Madrid and Ryan Heller and Shirsendu Nanda and Danush Shekar and Claudio San Martín and Matías Barría and Artur Apresyan and Zhenyu Ye and William K. Brooks and Wei Chen and Gabriele D'Amen and Gabriele Giacomini and Alessandro Tricoli and Aram Hayrapetyan and Hakseong Lee and Ohannes Kamer Köseyan and Sergey Los and Koji Nakamura and Sayuka Kita and Tomoka Imamura and Cristían Peña and Si Xie, "Results for pixel and strip centimeter-scale AC-LGAD sensors with a 120 GeV proton beam," 7 2024.

[3] M. Tabata *et al.*, "Silica aerogel radiator for use in the A-RICH system utilized in the Belle II experiment," *Nucl. Instrum. Meth. A*, vol. 766, pp. 212–216, 2014.

[4] R. Brun and F. Rademakers, "ROOT: An object oriented data analysis framework," *Nucl. Instrum. Meth. A*, vol. 389, pp. 81–86, 1997.

[5] J. de Favereau, C. Delaere, P. Demin, A. Giammanco, V. Lemaître, A. Mertens, and M. Selvaggi, "Delphes 3: a modular framework for fast simulation of a generic collider experiment," *Journal of High Energy Physics*, vol. 2014, Feb. 2014.

[6] F. T. Acosta, B. Karki, P. Karande, A. Angerami, M. Arratia, K. Barish, R. Milton, S. Morán, B. Nachman, and A. Sinha, "The optimal use of segmentation for sampling calorimeters," *JINST*, vol. 19, no. 06, p. P06002, 2024.

[7] M. M. David Ruth, Alex Jentsch, "Advanced methods for roman pots reconstruction at the eic." https://indico.cern.ch/event/1199314/contributions/5193191/attachments/2619028/4527696/DIS_RNDtalk_DRuth.pdf, 2023.

[8] M. Tabata, I. Adachi, H. Kawai, T. Sumiyoshi, and H. Yokogawa, "Hydrophobic silica aerogel production at kek," *Nuclear Instruments and Methods in Physics Research Section A: Accelerators, Spectrometers, Detectors and Associated Equipment*, vol. 668, pp. 64–70, 2012.

[9] R. Abdul Khalek *et al.*, "Science Requirements and Detector Concepts for the Electron-Ion Collider: EIC Yellow Report," *Nucl. Phys. A*, vol. 1026, p. 122447, 2022.

[10] A. Accardi *et al.*, "Electron Ion Collider: The Next QCD Frontier: Understanding the glue that binds us all," *Eur. Phys. J. A*, vol. 52, no. 9, p. 268, 2016.

[11] A. Accardi *et al.*, "Electron Ion Collider: The Next QCD Frontier: Understanding the glue that binds us all," *Eur. Phys. J. A*, vol. 52, no. 9, p. 268, 2016.

[12] "National Academies of Sciences, Engineering, and Medicine, An Assessment of U.S.-Based Electron-Ion Collider Science," *The National Academies Press,Washington, DC*, 2018.

[13] J. K. Adkins *et al.*, "Design of the ECCE Detector for the Electron Ion Collider," 9 2022.

[14] J. Adam *et al.*, "ATHENA detector proposal — a totally hermetic electron nucleus apparatus proposed for IP6 at the Electron-Ion Collider," *JINST*, vol. 17, no. 10, p. P10019, 2022.

[15] M. Arratia, D. Britzger, O. Long, and B. Nachman, "Reconstructing the kinematics of deep inelastic scattering with deep learning," *Nucl. Instrum. Meth. A*, vol. 1025, p. 166164, 2022.

[16] A. MetZhao:2016rfuz and A. Vossen, "Parton Fragmentation Functions," *Prog. Part. Nucl. Phys.*, vol. 91, pp. 136–202, 2016.

[17] P. J. Mulders and R. D. Tangerman, "The Complete tree level result up to order 1/Q for polarized deep inelastic leptoproduction," *Nucl. Phys. B*, vol. 461, pp. 197–237, 1996. [Erratum: Nucl.Phys.B 484, 538–540 (1997)].

[18] A. Bacchetta, M. Diehl, K. Goeke, A. Metz, P. J. Mulders, and M. Schlegel, "Semi-inclusive deep inelastic scattering at small transverse momentum," *JHEP*, vol. 02, p. 093, 2007.

[19] D. W. Sivers, "Single Spin Production Asymmetries from the Hard Scattering of Point-Like Constituents," *Phys. Rev. D*, vol. 41, p. 83, 1990.

[20] D. W. Sivers, "Hard scattering scaling laws for single spin production asymmetries," *Phys. Rev. D*, vol. 43, pp. 261–263, 1991.

[21] E. C. Aschenauer, V. Batozskaya, S. Fazio, K. Gates, H. Moutarde, D. Sokhan, H. Spiesberger, P. Sznajder, and K. Tezgin, "EpIC: novel Monte Carlo generator for exclusive processes," *Eur. Phys. J. C*, vol. 82, no. 9, p. 819, 2022.

[22] D. Boer *et al.*, "Physics case for quarkonium studies at the Electron Ion Collider," 9 2024.

[23] L. Frankfurt, M. Strikman, and M. Zhalov, "Elastic and large t rapidity gap vector meson production in ultraperipheral proton–ion collisions," *Physics Letters B*, vol. 640, no. 4, pp. 162–169, 2006.

[24] A. Tumasyan, W. Adam, and Others, "Probing small bjorken-x nuclear gluonic structure via coherent j/ψ photoproduction in ultraperipheral pb-pb collisions at $\sqrt{s_{\mathrm{NN}}} = 5.02$ TeV," *Phys. Rev. Lett.*, vol. 131, p. 262301, Dec 2023.

[25] A. Baltz, G. Baur, D. d'Enterria, L. Frankfurt, F. Gelis, V. Guzey, K. Hencken, Y. Kharlov, M. Klasen, S. Klein, V. Nikulin, J. Nystrand, I. Pshenichnov, S. Sadovsky, E. Scapparone, J. Seger, M. Strikman, M. Tverskoy, R. Vogt, S. White, U. Wiedemann, P. Yepes, and M. Zhalov, "The physics of ultraperipheral collisions at the lhc," *Physics Reports*, vol. 458, no. 1, pp. 1–171, 2008.

[26] J.-P. Lansberg, K. Lynch, C. Van Hulse, and R. McNulty, "Inclusive photoproduction of vector quarkonium in ultra-peripheral collisions at the LHC," 9 2024.

[27] S. R. Klein and H. Mäntysaari, "Imaging the nucleus with high-energy photons," *Nature Rev. Phys.*, vol. 1, no. 11, pp. 662–674, 2019.

[28] K. J. Eskola, C. A. Flett, V. Guzey, T. Löytäinen, and H. Paukkunen, "Exclusive quarkonium photoproduction in A+A UPCs at the LHC in NLO pQCD," *PoS*, vol. HardProbes2023, p. 107, 2024.

[29] C. A. Flett, J. P. Lansberg, S. Nabeebaccus, M. Nefedov, P. Sznajder, and J. Wagner, "Exclusive vector-quarkonium photoproduction at NLO in alpha_s in collinear factorisation with evolution of the generalised parton distributions and high-energy resummation," 9 2024.

[30] S. R. Klein, J. Nystrand, J. Seger, Y. Gorbunov, and J. Butterworth, "Starlight: A monte carlo simulation program for ultra-peripheral collisions of relativistic ions," *Computer Physics Communications*, vol. 212, pp. 258–268, 2017.

[31] Y. X. Zhao, A. Deshpande, J. Huang, K. S. Kumar, and S. Riordan, "Neutral-Current Weak Interactions at an EIC," *Eur. Phys. J. A*, vol. 53, no. 3, p. 55, 2017.

[32] "Radiation Doses." https://wiki.bnl.gov/EPIC/index.php?title=Radiation_Doses.

[33] S. Agostinelli *et al.*, "GEANT4—a simulation toolkit," *Nucl. Instrum. Meth. A*, vol. 506, p. 250, 2003.

[34] "The electron-ion collider user group.".

[35] R. A. Khalek *et al.*, "Science Requirements and Detector Concepts for the Electron-Ion Collider: EIC Yellow Report," *Nucl. Instr. and Meth. A*, vol. 1026, p. 122447, 2022.

[36] "The epic collaboration website.".

[37] A. Collaboration, "Technical Design report for the ALICE Inner Tracking System 3 - ITS3 ; A bent wafer-scale monolithic pixel detector," tech. rep., CERN, Geneva, 2024.

[38] M. Karagounis, D. Arutinov, M. Barbero, F. Huegging, H. Krueger, and N. Wermes, "An integrated shunt-ldo regulator for serial powered systems," in *2009 Proceedings of ESSCIRC*, pp. 276–279, 2009.

[39] A. Paramonov, "FELIX: the Detector Interface for the ATLAS Experiment at CERN," *EPJ Web Conf.*, vol. 251, p. 04006, 2021.

[40] lpGBT Design Team, "lpgbt documentation – release," 2024.

[41] J. Troska *et al.*, "The VTRx+, an optical link module for data transmission at HL-LHC," 2017.

[42] D. Higinbotham and et *al*., "Science requirements and detector concepts for the electron-ion collider: Eic yellow report," *Nuclear Physics A*, vol. 1026, p. 122447, 2022.

[43] F. Willeke and J. Beebe-Wang, "Electron ion collider conceptual design report 2021," 2 2021.

[44] ePIC, "Summary of epic background rates," 2024.

[45] EIC, "Eic detector geometry," 2024.

[46] D. Neyret, P. Abbon, M. Anfreville, V. Andrieux, Y. Bedfer, D. Durand, S. Herlant, N. d'Hose, F. Kunne, S. Platchkov, F. Thibaud, M. Usseglio, and M. Vandenbroucke, "Aging effects in the compass hybrid gem-micromegas pixelized detectors," *Nuclear Instruments and Methods in Physics Research Section A: Accelerators, Spectrometers, Detectors and Associated Equipment*, vol. 1065, p. 169511, 2024.

[47] C. Altunbas, M. Capeans, K. Dehmelt, J. Ehlers, J. Friedrich, I. Konorov, A. Gandi, S. Kappler, B. Ketzer, R. De Oliveira, S. Paul, A. Placci, L. Ropelewski, F. Sauli, F. Simon, and M. van Stenis, "Construction, test and commissioning of the triple-gem tracking detector for compass," *Nuclear Instruments and Methods in Physics Research Section A: Accelerators, Spectrometers, Detectors and Associated Equipment*, vol. 490, no. 1, pp. 177–203, 2002.

[48] T. Kawamoto *et al.*, "New Small Wheel Technical Design Report," *CERN-LHCC-2013-006, ATLAS-TDR-020, CERN-LHCC-2013-006, ATLAS-TDR-020*, 6 2013.

[49] M. Poli Lener, G. Bencivenni, R. de Olivera, G. Felici, S. Franchino, M. Gatta, M. Maggi, G. Morello, and A. Sharma, "The μ-rwell: A compact, spark protected, single amplification-stage mpgd," *Nuclear Instruments and Methods in Physics Research Section A: Accelerators, Spectrometers, Detectors and Associated Equipment*, vol. 824, pp. 565–568, 2016. Frontier Detectors for Frontier Physics: Proceedings of the 13th Pisa Meeting on Advanced Detectors.

[50] E. Farina, B. A. Gonzalez, P. Iengo, L. Longo, J. Samarati, G. Sekhniaidze, O. Sidiropoulou, and J. Wotschack, "Resistive micromegas high-rate and long-term ageing studies at the cern gamma irradiation facility," *Nuclear Instruments and Methods in Physics Research Section A: Accelerators, Spectrometers, Detectors and Associated Equipment*, vol. 1042, p. 167423, 2022.

[51] M. Chefdeville and et *al.*, "Development of micromegas detectors with resistive anode pads," *Nuclear Instruments and Methods in Physics Research Section A: Accelerators, Spectrometers, Detectors and Associated Equipment*, vol. 1003, p. 165268, 2021.

[52] L. Shekhtman, G. Fedotovich, A. Kozyrev, V. Kudryavtsev, T. Maltsev, and A. Ruban, "Development of μrwell detectors for the upgrade of the tracking system of cmd-3 detector," *Nuclear Instruments and Methods in Physics Research Section A: Accelerators, Spectrometers, Detectors and Associated Equipment*, vol. 936, pp. 401–404, 2019.

[53] A. Acker, D. Attié, S. Aune, J. Ball, P. Baron, Q. Bertrand, D. Besin, T. Bey, F. Bossù, R. Boudouin, M. Boyer, G. Christiaens, P. Contrepois, M. Defurne, E. Delagnes, M. Garçon, F. Georges, J. Giraud, R. Granelli, N. Grouas, C. Lahonde-Hamdoun, T. Lerch, I. Mandjavidze, O. Meunier, Y. Moudden, S. Procureur, M. Riallot, F. Sabatié, M. Vandenbroucke, and E. Virique, "The clas12 micromegas vertex tracker," *Nuclear Instruments and Methods in Physics Research Section A: Accelerators, Spectrometers, Detectors and Associated Equipment*, vol. 957, p. 163423, 2020.

[54] I. Giomataris, R. De Oliveira, S. Andriamonje, S. Aune, G. Charpak, P. Colas, A. Giganon, P. Rebourgeard, and P. Salin, "Micromegas in a bulk," *Nucl. Instrum. Meth. A*, vol. 560, pp. 405–408, 2006.

[55] H. Schindler and R. Veenhof, "Garfield++," 2024.

[56] K. Gnanvo and et *al.*, "Development of double-sided thin-gap gem-μrwell for tracking at the eic." https://www.jlab.org/sites/default/files/eic_rd_prgm/files/2023_Proposals/20230714_eRD_tgMPGD_Proposal_FY23_Final_EICGENRandD2023_16.pdf, 2023.

[57] K. Gnanvo, N. Liyanage, B. Mehl, and R. de Oliveira, "Performance of a resistive micro-well detector with capacitive-sharing strip anode readout," *Nuclear Instruments and Methods in Physics Research Section A: Accelerators, Spectrometers, Detectors and Associated Equipment*, vol. 1047, p. 167782, 2023.

[58] M. Calvi, P. Carniti, C. Gotti, C. Matteuzzi, and G. Pessina, "Single photon detection with SiPMs irradiated up to 10^{14} cm^{-2} 1-MeV-equivalent neutron fluence," *Nucl. Instrum. Meth. A*, vol. 922, pp. 243–249, 2019.

[59] "Technical Design Report: A High-Granularity Timing Detector for the ATLAS Phase-II Upgrade," tech. rep., CERN, Geneva, 2020.

[60] C. Madrid, R. Heller, C. San Martín, S. Nanda, A. Apresyan, W. Brooks, W. Chen, G. Giacomini, O. Kamer Köseyan, S. Los, C. Peña, R. Rios, A. Tricoli, S. Xie, and Z. Ye, "First survey of centimeter-scale ac-lgad strip sensors with a 120 gev proton beam," *Journal of Instrumentation*, vol. 18, p. P06013, June 2023.

[61] C. Bishop, A. Das, J. Ding, M. Gignac, F. Martinez-McKinney, S. Mazza, A. Molnar, N. Nagel, M. Nizam, J. Ott, H.-W. Sadrozinski, B. Schumm, A. Seiden, T. Shin, A. Summerell, M. Wilder, and Y. Zhao, "Long-distance signal propagation in ac-lgad," *Nuclear Instruments and Methods in Physics Research Section A: Accelerators, Spectrometers, Detectors and Associated Equipment*, vol. 1064, p. 169478, 2024.

[62] L. Menzio *et al.*, "First test beam measurement of the 4D resolution of an RSD pixel matrix connected to a FAST2 ASIC," *Nucl. Instrum. Meth. A*, vol. 1065, p. 169526, 2024.

[63] S. Xie, A. Apresyan, R. Heller, C. Madrid, I. Dutta, A. Hayrapetyan, S. Los, C. Peña, and T. Zimmerman, "Design and performance of the fermilab constant fraction discriminator asic," *Nuclear Instruments and Methods in Physics Research Section A: Accelerators, Spectrometers, Detectors and Associated Equipment*, vol. 1056, p. 168655, 2023.

[64] J. D. Brandenburg *et al.*, "The STAR Forward Silicon Tracker," 7 2024.

[65] C. Chock, K. Flood, L. Macchiarulo, F. Martinez-Mckinney, A. Martinez-Rojas, S. Mazza, I. Mostafanezhad, M. Nizam, J. Ott, R. Perron, E. Ryan, H.-W. Sadrozinski, B. Schumm, A. Seiden, K. Shin, M. Tarka, D. Uehara, M. Wilder, and Y. Zhao, "First test results of the transimpedance amplifier stage of the ultra-fast hpsoc asic," *Journal of Instrumentation*, vol. 18, p. C02016, feb 2023.

[66] O. H. W. Siegmund *et al.*, "Advances in microchannel plates and photocathodes for ultraviolet photon counting detectors," *Society of Photo-Optical Instrumentation Engineers Proceedings*, vol. 81450J.

[67] C. J. Hamel *et al.*, "LAPPD and HRPPD: Upcoming Upgrades to Incom's Fast Photosensors,"

[68] "Popecki." https://indico.cfnssbu.physics.sunysb.edu/event/265/contributions/922/attachments/261/411/LAPPD%20and%20HRPPD%20update%20EIC%20Workshop%2005-08-2024.pptx.

[69] J. A. et al, "Performance of an LAPPD in magnetic fields," *Nucl.Instrum.Meth. A*, no. 1072, p. 170122, 2025.

[70] "EICROC ASIC." https://indico.bnl.gov/event/18539/contributions/73731/attachments/46348/78403/CdLT_EICROC_6mar23.pdf.

[71] "Organization for Micro-Electronics desiGn and Applications." https://portail.polytechnique.edu/omega/.

[72] J. Anderson *et al.*, "FELIX: a PCIe based high-throughput approach for interfacing front-end and trigger electronics in the ATLAS Upgrade framework," *JINST*, vol. 11, no. 12, p. C12023, 2016.

[73] "Chiba Aerogel Factory Co., Ltd.." https://www.aerogel-factory.jp/.

[74] M. Yonenaga *et al.*, "Performance evaluation of the aerogel RICH counter for the Belle II spectrometer using early beam collision data," *Prog. Theor. Exp. Phys.*, no. 093H01, 2020.

[75] "ePIC IRT Package." https://github.com/eic/irt/tree/pfrich.

[76] R. Brun and F. Rademakers, "ROOT - An Object Oriented Data Analysis Framework, Proceedings AIHENP'96 Workshop, Lausanne," *Nucl. Inst. & Meth. in Phys. Res. A*, no. 389, pp. 81–86, 1997.

[77] M. Tabata, I. Adachi, Y. Hatakeyama, H. Kawai, T. Morita, and T. Sumiyoshi, "Large-area silica aerogel for use as cherenkov radiators with high refractive index, developed by supercritical carbon dioxide drying," *The Journal of Supercritical Fluids*, vol. 110, pp. 183–192, 2016.

[78] "CAEN A1515BV 16-channel floating ground High Voltage module." https://www.caen.it/products/a1515b/.

[79] "CAEN SY4527 High Voltage mainframe." https://www.caen.it/products/SY4527/.

[80] "Wiener Mpod Low Voltage system." https://www.wiener-d.com/power-supplies/mpod-lv-hv/.

[81] A. Buzykaev, A. Danilyuk, S. Ganzhur, E. Kravchenko, and A. Onuchin, "Measurement of optical parameters of aerogel," *Nuclear Instruments and Methods in Physics Research Section A: Accelerators, Spectrometers, Detectors and Associated Equipment*, vol. 433, no. 1, pp. 396–400, 1999.

[82] A. J. Hunt, "Light scattering for aerogel characterization," *Journal of Non-Crystalline Solids*, vol. 225, pp. 303–306, 1998.

[83] S. K. Sahu *et al.*, "Measurement of Radiation Damage on Silica Aerogel Cherenkov Radiator," *Nucl. Instrum. Meth. A*, vol. 382, pp. 441–446, 1996.

[84] R. Abjean, A. Bideau-Mehu, and Y. Guern, "Refractive index of hexafluoroethane (C-2F-6) in the 300-nm to 150-nm wavelength range," *Nucl. Instrum. Meth. A*, vol. 354, pp. 417–418, 1995.

[85] C. Piemonte and A. Gola, "Overview on the main parameters and technology of modern Silicon Photomultipliers," *Nucl. Instrum. Meth. A*, vol. 926, pp. 2–15, 2019.

[86] L. P. Rignanese, P. Antonioli, R. Preghenella, and E. Scapparone, "SiPMs and examples of applications for low light detection in particle and astroparticle physics," *Riv. Nuovo Cim.*, vol. 47, no. 5, pp. 299–349, 2024. [Erratum: Riv.Nuovo Cim. 47, (2024)].

[87] S. España, L. Fraile, J. Herraiz, J. Udías, M. Desco, and J. Vaquero, "Performance evaluation of sipm photodetectors for pet imaging in the presence of magnetic fields," *Nuclear Instruments and Methods in Physics Research Section A: Accelerators, Spectrometers, Detectors and Associated Equipment*, vol. 613, no. 2, pp. 308–316, 2010.

[88] F. Acerbi *et al.*, "Cryogenic Characterization of FBK HD Near-UV Sensitive SiPMs," *IEEE Trans. Electron. Dev.*, vol. 64, pp. 521–526, 10 2016.

[89] S. Merzi, F. Acerbi, C. Aicardi, D. Fiore, V. Goiffon, A. G. Gola, O. Marcelot, A. Materne, and O. Saint-Pe, "Radiation Damage on Silicon Photomultipliers from Ionizing and Non-Ionizing Radiation of Low-Earth Orbit Operations," *Sensors*, vol. 24, no. 15, p. 4990, 2024.

[90] E. Garutti and Y. Musienko, "Radiation damage of SiPMs," *Nucl. Instrum. Meth. A*, vol. 926, pp. 69–84, 2019.

[91] T. Tsang, T. Rao, S. Stoll, and C. Woody, "Neutron radiation damage and recovery studies of SiPMs," *JINST*, vol. 11, no. 12, p. P12002, 2016.

[92] EU, "Regulation (EU) 2024/573 of the European Parliament and of the Council on fluorinate greehouse gases," *https://eur-lex.europa.eu/eli/reg/2024/573/oj*, 2024.

[93] E. Nappi, "Aerogel and its applications to rich detectors," *Nuclear Physics B - Proceedings Supplements*, vol. 61, no. 3, pp. 270–276, 1998. Proceedings of the Fifth International Conference on Advanced Technology and Particle Physics.

[94] M. Kubantsev, I. Larin, and A. Gasparian, "Performance of the PrimEx electromagnetic calorimeter," *AIP Conf. Proc.*, vol. 867, no. 1, pp. 51–58, 2006.

[95] T. Horn *et al.*, "Scintillating crystals for the Neutral Particle Spectrometer in Hall C at JLab," *Nucl. Instrum. Meth. A*, vol. 956, p. 163375, 2020.

[96] A. Asaturyan *et al.*, "Electromagnetic calorimeters based on scintillating lead tungstate crystals for experiments at Jefferson Lab," *Nucl. Instrum. Meth. A*, vol. 1013, p. 165683, 2021.

[97] F. Ameli *et al.*, "Streaming readout for next generation electron scattering experiments," *Eur. Phys. J. Plus*, vol. 137, no. 8, p. 958, 2022.

[98] T. D. Beattie *et al.*, "Construction and Performance of the Barrel Electromagnetic Calorimeter for the GlueX Experiment," *Nucl. Instrum. Meth. A*, vol. 896, pp. 24–42, 2018.

[99] Y. Suda *et al.*, "Performance evaluation of the high-voltage CMOS active pixel sensor AstroPix for gamma-ray space telescopes," *Nucl. Instrum. Meth. A*, vol. 1068, p. 169762, 2024.

[100] ePIC Collaboration, "Background studies - epic." https://wiki.bnl.gov/EPIC/index.php?title=Background, 2023. Accessed: 2024-09-28.

[101] O. D. Tsai *et al.*, "Results of \& on a new construction technique for W/ScFi Calorimeters," *J. Phys. Conf. Ser.*, vol. 404, p. 012023, 2012.

[102] C. A. Aidala *et al.*, "Design and Beam Test Results for the sPHENIX Electromagnetic and Hadronic Calorimeter Prototypes," *IEEE Trans. Nucl. Sci.*, vol. 65, no. 12, pp. 2901–2919, 2018.

[103] T. Nicholls *et al.*, "Performance of an electromagnetic lead / scintillating fiber calorimeter for the H1 detector," *Nucl. Instrum. Meth. A*, vol. 374, pp. 149–156, 1996.

[104] O. D. Tsai *et al.*, "Development of a forward calorimeter system for the STAR experiment," *J. Phys. Conf. Ser.*, vol. 587, no. 1, p. 012053, 2015.

[105] F. Aaron *et al.*, "Measurement of the proton structure function fl(x,q2) at low x," *Physics Letters B*, vol. 665, no. 4, pp. 139–146, 2008.

[106] R.-D. Appuhn *et al.*, "The h1 lead/scintillating-fibre calorimeter," *Nuclear Instruments and Methods in Physics Research Section A: Accelerators, Spectrometers, Detectors and Associated Equipment*, vol. 386, no. 2, pp. 397–408, 1997.

[107] "SiPM radiation hardness study." https://indico.bnl.gov/event/24087/#17-further-rad-hard-studies-an.

[108] A. White *et al.*, "Design, construction and commissioning of a technological prototype of a highly granular sipm-on-tile scintillator-steel hadronic calorimeter," *Journal of Instrumentation*, vol. 18, p. P11018, nov 2023.

[109] V. Andrieux, R. Nothnagel, C. Riedl, and D. Sharma, "Vector-meson reconstruction in the epic backward hcal," tech. rep., UIUC, nov 2024. https://doi.org/10.5281/zenodo.14200156.

[110] M. Salajegheh, H. Khanpour, U.-G. Meißner, H. Hashamipour, and M. Soleymaninia, "Determination of diffractive PDFs from a global QCD analysis of inclusive diffractive DIS and dijet cross-section measurements at HERA," *Phys. Rev. D*, vol. 107, no. 9, p. 094038, 2023.

[111] E. Meschi, T. Monteiro, C. Seez, and P. Vikas, "Electron Reconstruction in the CMS Electromagnetic Calorimeter," tech. rep., CERN, Geneva, 2001.

[112] "The algorithm for the PWO calorimeter." https://www.jlab.org/primex/weekly_meetings/primexII/slides_2012_01_20/island_algorithm.pdf.

[113] A. Laudrain and on behalf of the CALICE Collaboration, "The calice ahcal: a highly granular sipm-on-tile hadron calorimeter prototype," *Journal of Physics: Conference Series*, vol. 2374, p. 012017, nov 2022.

[114] "The Phase-2 Upgrade of the CMS Endcap Calorimeter," tech. rep., CERN, Geneva, 2017.

[115] M. Arratia *et al.*, "A high-granularity calorimeter insert based on SiPM-on-tile technology at the future Electron-Ion Collider," *Nucl. Instrum. Meth. A*, vol. 1047, p. 167866, 2023.

[116] M. Arratia, B. Bagby, P. Carney, J. Huang, R. Milton, S. J. Paul, S. Preins, M. Rodriguez, and W. Zhang, "Beam Test of the First Prototype of SiPM-on-Tile Calorimeter Insert for the EIC Using 4 GeV Positrons at Jefferson Laboratory," *Instruments*, vol. 7, no. 4, p. 43, 2023.

[117] S. J. Paul and M. Arratia, "Leveraging staggered tessellation for enhanced spatial resolution in high-granularity calorimeters," *Nucl. Instrum. Meth. A*, vol. 1060, p. 169044, 2024.

[118] M. Arratia, L. Garabito Ruiz, J. Huang, S. J. Paul, S. Preins, and M. Rodriguez, "Studies of time resolution, light yield, and crosstalk using SiPM-on-tile calorimetry for the future Electron-Ion Collider," *JINST*, vol. 18, no. 05, p. P05045, 2023.

[119] R. Milton, S. J. Paul, B. Schmookler, M. Arratia, P. Karande, A. Angerami, F. T. Acosta, and B. Nachman, "Design of a SiPM-on-Tile ZDC for the future EIC and its Performance with Graph Neural Networks," 5 2024.

[120] "Point Cloud Deep Learning Methods for Pion Reconstruction in the ATLAS Experiment," tech. rep., CERN, Geneva, 2022. All figures including auxiliary figures are available at https://atlas.web.cern.ch/Atlas/GROUPS/PHYSICS/PUBNOTES/ATL-PHYS-PUB-2022-040.

[121] S. Lai *et al.*, "Software Compensation for Highly Granular Calorimeters using Machine Learning," *JINST*, vol. 19, p. P04037, 2024.

[122] ePIC Collaboration, "Far-forward detectors - epic." https://wiki.bnl.gov/EPIC/index.php?title=FarForward, 2024. Accessed: 2024-12-06.

[123] E. C. Aschenauer, S. Fazio, G. Giacomini, A. Jentsch, A. Kiselev, and A. Tricoli, "Sensors for roman pots at the eic." https://indico.bnl.gov/event/7449/contributions/35871/attachments/27124/41452/Tricoli_Roman_Pots_EIC_TempleMgt_ACLGAD_march2020.pdf, 2020.

[124] "lpGBT Documentation."

[125] G. B. et al., "HGCROC-Si and HGCROC-SiPM: the front-end readout ASICs for the CMS HGCAL," in *IEEE Nuclear Science Symposium and Medical Imaging Conference (NSS/MIC)*, pp. 1–4, 2020.

[126] X. H. et al., "The testing and performance of the ETROC2 for CMS MTD Endcap Timing Layer (ETL) upgrade," in *2024 IEEE Nuclear Science Symposium (NSS), Medical Imaging Conference (MIC) and Room Temperature Semiconductor Detector Conference (RTSD)*, pp. 1–2, 2024.

[127] S. B. et al, "SAMPA chip: a new ASIC for the ALICE TPC and MCH upgrades.," *Journal of Instrumentation*, February 2016.

[128] A. Pilyar, "The 32-channel Readout Front end Card FEC32S based on SAMPA ASIC for the Dubna NICA TPC," in *2018 IEEE XXVII International Scientific Conference Electronics – ET*, pp. 1–3, 2018.

[129] J. Troska, A. Brandon-Bravo, S. Detraz, A. Kraxner, L. Olanterä, C. Scarcella, C. Sigaud, C. Soos, and F. Vasey, "The VTRx+, an optical link module for data transmission at HL-LHC," *PoS*, vol. TWEPP-17, p. 048, 2017.

[130] J. Anderson *et al.*, "FELIX: a PCIe based high-throughput approach for interfacing front-end and trigger electronics in the ATLAS Upgrade framework," *JINST*, vol. 11, no. 12, p. C12023, 2016.

[131] R. A. et al., "APEIRON: A framework for high level programming of dataflow applications on Multi-FPGA systems," *EPJ Web of Conferences*, no. 11002, 2024.